ACS APPLIED MATERIALS & INTERFACES

Research Article

www.acsami.org

Preparation of Well-Dispersed Gold/Magnetite Nanoparticles Embedded on Cellulose Nanocrystals for Efficient Immobilization of Papain Enzyme

Khaled A. Mahmoud,*[,†,‡] Edmond Lam,[‡] Sabahudin Hrapovic,[‡] and John H. T. Luong[‡]

[†]Qatar Environment and Energy Research Institute (QEERI), Qatar Foundation, P.O. Box 5825, Doha, Qatar

[‡]Building Montreal-Royalmount, Canada National Research Council, 6100 Royalmount Ave. Montreal, Quebec, Canada H4P 2R2

ABSTRACT: A nanocomposite consisting of magnetite nanoparticles (Fe_3O_4NPs) and Au nanoparticles (AuNPs) embedded on cellulose nanocrystals (CNCs) was used as a magnetic support for the covalent conjugation of papain and facilitated recovery of this immobilized enzyme. Fe_3O_4NPs (10−20 nm in diameter) and AuNPs (3−7 nm in diameter) were stable and well-dispersed on the CNC surface. Energy-dispersive spectroscopy, X-ray diffraction, and Fourier transform infrared spectroscopy were used to evaluate the surface composition and structure of CNC/Fe_3O_4NPs/AuNPs. The nanocomposite was successfully used for the immobilization and separation of papain from the reaction mixture. The optimal enzyme loading was 186 mg protein/g CNC/Fe_3O_4NPs/AuNPs, significantly higher than the value reported in the literature. The activity of immobilized papain was studied by electrochemical detection of its specific binding to the Thc-Fca-Gly-Gly-Tyr-Arg inhibitory sequence bound to an Au electrode. The immobilized enzyme retained 95% of its initial activity after 35 days of storage at 4 °C, compared to 41% for its free form counterpart.

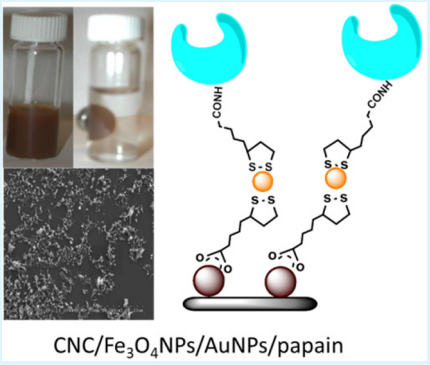

CNC/Fe_3O_4NPs/AuNPs/papain

KEYWORDS: *magnetite nanoparticles, gold nanoparticles, papain, enzyme immobilization, electrochemical detection*

INTRODUCTION

Magnetic nanoparticles (MNPs) have been used in the enzyme/protein support and biotechnological/biomedical fields to facilitate substrate and product recovery.[1−5] Target materials on MNPs are easily isolated from sample solutions under a magnetic field. This property has been exploited in large-scale processes for selective catalyst removal from the reaction mixture. However, the size control and dispersion of MNPs is an important issue because they often suffer from aggregation with diminishing magnetic properties when applied to complex environmental and biological systems.[6] Surface coating with a stabilizing agent is also required to stabilize the particles in aqueous media at certain concentrations.[7] There are several reports on the synthesis of magnetic core/shell nanoparticles with a magnetite (Fe_3O_4) core and a metal or metal oxide shell. In particular, Au nanoparticles (AuNPs) are promising materials for protecting Fe_3O_4 nanoparticles due to their simple reductive preparation, reliable chemical stability, biocompatibility, and versatility in surface modification.[8] Fe_3O_4/Au composites display different structures: core/shell Fe_3O_4/Au nanomaterials,[8,9] dumbbell-like Au−Fe_3O_4 nanoparticles,[10] and covalent attachment of AuNPs onto colloidal Fe_3O_4.[1]

Robust cellulose nanocrystals (CNCs) with biocompatibility, high crystallinity and mechanical tensile have been fostered in a myriad of applications including enzyme immobilization,[11] drug delivery,[12] and biomedical applications.[13,14] Conjugation of CNCs with nanomaterials has provided excellent hybrid supports for enzymes. AuNPs can be readily functionalized with thiolated molecules with carboxylic functional groups, which in-turn, are conjugated with amine groups of proteins/enzymes.[15−17] The CNC/AuNPs matrix can have significant biocatalytic activity with excellent stability and recovered specific activity (70−95%) for enzymes.[11]

This study describes the applicability of a CNC/Fe_3O_4NPs composite embedded with AuNPs (CNC/Fe_3O_4NPs/AuNPs) as a support for the immobilization and separation of papain from a solution. Although magnetic cellulosic nanocrystals have been described by Liu et al.[18] and Marchessault et al.,[19] this paper is the first demonstration for the preparation of magnetic CNCs with AuNPs for efficient enzyme immobilization. The size, structure, and magnetic properties of this matrix were evaluated before and after conjugation with papain as a model system. A selective electrochemical detection method, together with conventional enzyme assays, was used to evaluate the enzyme loading, storage stability and separation efficiency.

MATERIALS AND METHODS

Materials. Papain (EC 3.4.22.2), thioctic acid (Thc), sodium borohydride, gold(III) chloride, sodium phosphate monobasic, sodium phosphate dibasic, 2-(*N*-morpholino)ethanesulfonic acid (MES), 1-ethyl-3-(3-dimethylaminopropyl)carbodiimide (EDC), decanethiol, *N*-hydroxysulfosuccinimide (NHS), bovine serum albumin (BSA), Z-

Received: February 28, 2013
Accepted: May 15, 2013
Published: May 15, 2013

   dx.doi.org/10.1021/am4007534 | *ACS Appl. Mater. Interfaces* 2013, 5, 4978−4985

Scheme 1. Schematic Representation of the Stepwise Formation of the Conjugate of CNC/Fe_3O_4NPs/AuNPs/Papain[a]

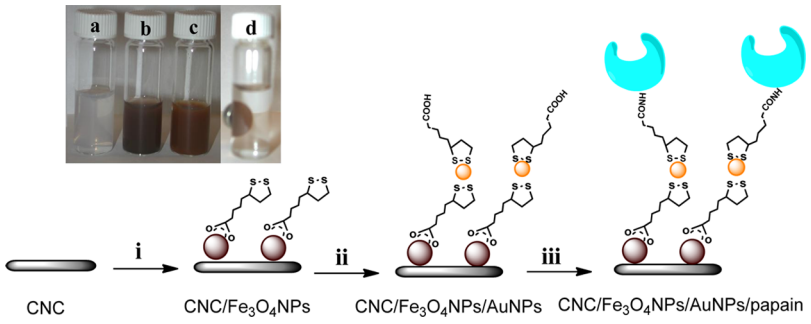

[a](i) $FeCl_3$, $FeCl_2$, thioctic acid; (ii) $HAuCl_4$, α-cyclodextrin, $NaBH_4$, thioctic acid; (iii) EDC, NHS, papain. Inset shows the photograph of (a) pristine CNC; (b) CNC/Fe_3O_4NPs; (c) CNC/Fe_3O_4NPs/AuNPs; and (d) CNC/Fe_3O_4NPs/AuNPs attracted to the side wall with a permanent magnet.

Phe-Arg-NHNp, and dithiothreitol (DTT) were purchased from Sigma-Aldrich. All analytical grade solvents were used without further purification. The Thc-Fca-Gly-Gly-Tyr-Arg peptide was prepared as described elsewhere.[20]

Preparation of CNCs/Fe_3O_4NPs. The preparation of CNCs was described in detail elsewhere.[11] Fe_3O_4NPs were synthesized under argon by coprecipitation of $FeCl_3{\cdot}6H_2O$ (3.2 mmol) and $FeCl_2{\cdot}4H_2O$ (1.6 mmol) in a 1% CNC aqueous suspension with ammonium hydroxide (0.65 mL, 28%) and thioctic acid (9.2 mmol) at room temperature. After heating at 80 °C for 2 h, the resulting precipitate was purified by washing and subjected to magnetic separation three times by using a neodymium disk (12.6 mm) magnet (axially magnetized, model ZD3, pull force 7.74 lbs, surface field 3761 G; K&J Magnetics Inc.).

Preparation of CNCs/Fe_3O_4NPs/AuNPs. AuNPs were synthesized in situ in the presence of CNCs/Fe_3O_4NPs as described in Scheme 1.[11] $HAuCl_4$ (10 mM, 1.6 mL) and α-cyclodextrin (2 mM, 2 mL) were added to CNC/Fe_3O_4NPs (23 mg/mL, 4 mL). Freshly prepared, ice-cold 0.1 M $NaBH_4$ was added in five aliquots (20 μL) to a slowly mixing solution of gold salt and CNC/Fe_3O_4NPs until a stable reddish black colloid was obtained. After being left at room temperature for 24 h, the CNC/Fe_3O_4NPs/AuNPs colloid was washed three times by the separation of CNC/Fe_3O_4NPs/AuNPs conjugate form the solution mixture using a strong magnet to remove any unbound AuNPs. It should be noted that the supernatant was clear after the first washing cycle.

Film Characterization. A Hitachi scanning electron microscope (SEM, S-2600N, Tokyo, Japan) was used for topographical analysis of the nanocomposite. The SEM was equipped with an energy-dispersive X-ray (EDX) spectrometer, and a LN_2-free analytical silicon drift detector (INCA x-act, Oxford Instruments, UK). The SEM/EDX system was operated with a high vacuum mode at 10−15 kV, emission current of 20−40 μA, and a working distance of 3−10 mm. EDX has software with a database of reference spectra for elemental analysis, compositional nanoanalysis and mapping. A drop of nanomaterial was dried on a silica plate and introduced into the chamber. Low voltage transmission electron microscopy (LVTEM) micrographs were obtained by a Delong LVEM, low voltage electron microscope (Soquelec, Montreal, QC, Canada) operating in TEM mode at 5 kV. A 5 μL drop of well-dispersed suspension was then dried on a 300 mesh, Cu-300CN grid (Pacific Grid-Tech) and analyzed. High-resolution transmission electron microscope (HRTEM) micrographs were obtained by a Hitachi TEM (model H-7500, Tokyo, Japan) at 60 and 80 kV. A small amount of sample was suspended in methanol and sonicated to disperse the material. A 20 μL drop of well-dispersed suspension was then dried on a Formvar-carbon coated grid and analyzed. Fourier transform infrared (FTIR) spectra were collected from 4000 to 400 cm^{-1} for 64 scans at a resolution of 4 cm^{-1} using a Bruker Tensor 27 FTIR spectrophotometer. Cyclic voltammetry (CV) and differential pulse voltammetry (DPV) were performed using an electrochemical analyzer coupled with a picoamp booster and a Faraday cage (CHI 760B, CH Instruments, Austin, TX). A Pt wire (Aldrich, 99.9% purity, 1 mm diameter) and an Ag/AgCl, 3 M NaCl (BAS, West Lafayette, IN) electrode were used as counter and reference electrodes, respectively. Au disk electrodes were polished with polishing paper (grid 2000) and subsequently with alumina until a mirror finish was obtained. The electrodes were sonicated for 5 min to remove alumina residues followed by thorough rinsing with deionized water and ethanol, respectively. The electrodes were conditioned by CV between 0 and +1.4 V vs Ag/AgCl at 100 mV s^{-1} in 0.5 M H_2SO_4 until a stable CV profile was obtained. Powder X-ray diffraction (PXRD) patterns were measured using monochromatized Co Kα (λ = 1.79021 Å) radiation on a Rigaku X-ray diffractometer (model, RAD-R, The Woodlands, TX). The PXRD profile data were collected at every 0.04° over the range of 5−80° in 2θ with a scanning speed of 0.5°/min. The magnetic properties of the composite were measured on a vibrating sampling magnetometer (VSM) 7307 (Lakeshore Cryotronic, Westerville, OH)

Surface Activation of the Nanocomposite. CNC/Fe_3O_4NPs/AuNPs colloids were separated with a strong magnet and the pellet was resuspended in ethanol. This step was repeated three times. The material was stirred in an ethanol solution containing 0.05 M thioctic acid (Thc) for 24 h. Thc was covalently attached to AuNPs through the Au−S "self-assembled" bond formation.

Enzyme Immobilization on an Activated Nanocomposite. The conjugation of papain onto the activated nanocomposite surface was performed using a two-step carbodiimide coupling protocol.[11] CNC/Fe_3O_4NPs/AuNPs (50 mg/mL) were suspended in 0.05 M MES, 0.5 M NaCl buffer, pH 5.7 (5 mL) prior to the addition of 5 mM EDC and 10 mM NHS. The suspension was stirred for 30 min at room temperature. NHS activation was confirmed by FTIR spectroscopy upon analysis of freeze-dried samples of the conjugate. The activated material was recovered by placing the reaction mixture over a strong magnet and washed three times with deionized water. The CNC/Fe_3O_4NPs/AuNPs conjugate (10, 25, 50 mg/mL) was then transferred to vials containing purified papain (0.1−6.4 mg/mL) in 0.1 M phosphate buffer with 0.5 M NaCl (at pH 7.2, room temperature) to determine the maximal binding capacity of the modified CNC. After 2 h, the samples were separated with a magnet and the supernatants from three washes were collected for quantification of the enzyme binding efficiency.

Enzyme Binding Efficiency. The protein content in the collected supernatant was determined by a colorimetric method at λ = 595 nm with the Biorad Protein Assay Reagent Concentrate using bovine serum albumin (BSA) as the protein standard. The amount of bound enzymes was calculated as $(C_i - C_s)V$, where C_i and C_s are the concentration of the enzyme initially added for attachment and in the supernatant, respectively (mg/mL), and V is the reaction volume (mL).

Electrochemical Measurements of Enzyme Activity. A papain stock solution was prepared in 1 mM HCl. For daily activation, the papain stock solution was diluted in 0.1 M sodium phosphate pH 6.5,

containing 2.5 mM EDTA and 15 mM DTT, and then incubated at 23 °C for 1 h. The activated enzyme was kept on ice. The peptide film was immobilized by soaking Au disk electrodes in a 1 mM solution of the disulfide-terminated Thc-Fca-Gly-Gly-Tyr-Arg peptide for 24 h. The resulting film was then immersed in an ethanol solution containing 1 mM decanethiol for 2 min. The electrochemical detection of the CNC/Fe_3O_4NPs/AuNPs/papain conjugate was followed by recording the cyclic and differential pulse voltammograms (CV and DPV) due to the specific binding to the peptide films. All measurements were recorded in aqueous solutions of 2 M $NaClO_4$ containing papain activation buffer, with an Ag/AgCl reference electrode and a Pt wire counter electrode. The electrochemical assay for in situ enzyme separation was carried out by recording the CV or DPV of the peptide-modified electrode in a 2 M $NaClO_4$ aqueous solution containing the surface activated magnetite nanocomposite. Papain (0.1−6.4 mg/mL) was then added to the solution and allowed to react at pH 6.4 for 1 h before recording another CV or DPV. The electrochemical cell was placed over a magnet to separate the magnetic matrix with the bound enzyme, and another CV or DPV was recorded afterward.

Enzyme Activity Assay. The catalytic activity of CNC/Fe_3O_4NPs/AuNPs/papain was assayed at 23 °C with the chromogenic substrate Z-Phe-Arg-NHNp (200 μM). The buffer solution used for the assay was 0.1 M sodium phosphate pH 6.2, 2.5 mM EDTA, 300 μM DTT, and 30% DMSO. The reaction was initiated by 20 μL of the enzyme to catalyze the substrate at 1−2 μM/min. The reaction mixture was adjusted to a 1 mL volume. The concentration of liberated *p*-nitroaniline (*p*NA) was monitored over 10 min by measuring the absorbance at 405 nm (absorption coefficient of ε = 9.96 $cm^2/\mu mol$) against a blank sample containing enzyme free CNC/Fe_3O_4NPs/AuNPs. Rates were determined by duplicate measurements. A control assay was performed to determine the activity of the free enzyme at the same concentration which sets the activity as 100%. One unit is defined as that amount of sample which causes the decomposition of 1 pmol of substrate per min in the assay. A Lineweaver−Burk plot was constructed for determining the Michaelis−Menten constant (K_m).

Immobilized Enzyme Recovery and Reuse. The reusability of immobilized papain on CNC/Fe_3O_4NPs/AuNPs was studied under the same conditions as described in the activity assay section. After each run, CNC/Fe_3O_4NPs/AuNPs/papain was magnetically separated and washed with ultrapure water to remove any remaining products or substrate species. The residual enzyme activity after each cycle was normalized to the initial value of 100%

RESULTS AND DISCUSSION

Preparation and characterization of the magnetite nanocomposite. Scheme 1 summarizes the preparation of magnetically active CNC and its conjugation to papain as an activated matrix. The off-white CNC suspension was extracted from flax fibers by a modified acid hydrolysis method[11] using an acid-peroxide composition of 65% H_2SO_4:65% HNO_3:35% H_2O_2, 3:1:2. The method produced individual and aggregated rodlike crystalline cellulose fragments, ranging from 10−20 nm in diameter with a corresponding length of 120−300 nm. Fe_3O_4NPs were deposited on the CNC surface by coprecipitation of $FeCl_3/FeCl_2$ (2:1) with ammonium hydroxide in the presence of thioctic acid (Thc) to impart carboxylic acid functional groups on the surface of the Fe_3O_4NPs. CNCs served as a support matrix to control the growth of uniform Fe_3O_4NPs (10−15 nm), which exhibited superparamagnetic properties at room temperature with a saturation magnetization value as high as 60 emu/g.[1] FTIR was used to determine the presence of characteristic functional groups of each product over the course of the conjugate synthesis (Figure 1). FTIR features for the CNC include 3425 cm^{-1} (ν_{OH}), 2916 cm^{-1} (ν_{CH_2}), 1730 cm^{-1} ($\nu_{C=O}$), 1162 cm^{-1} (ν_{C-O-C}), 1112 cm^{-1} ($\nu_{Asym\ Ring}$), 1060 and 1034 cm^{-1} (ν_{C-O}), 664 cm^{-1} (ν_{C-OH}),

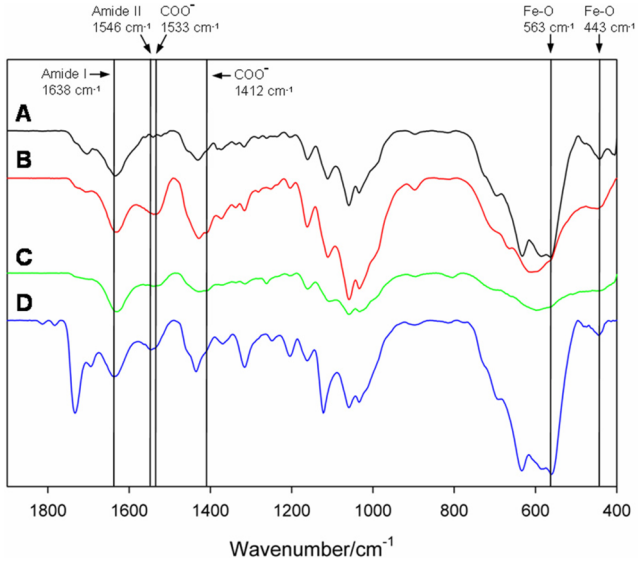

Figure 1. FTIR spectra of (A) CNC/Fe_3O_4NPs, (B) CNC/Fe_3O_4NPs reacted with Thc, (C) CNC/Fe_3O_4NPs/AuNPs, and (D) CNC/Fe_3O_4NPs/AuNPs/papain.

and 633 cm^{-1} (ν_{C-C-O}). Peaks at 443 and 563 cm^{-1} in the spectrum of CNC/Fe_3O_4NPs correspond to the Fe−O stretching of the magnetite.[21] Upon the addition of the first excess of Thc to CNC/Fe_3O_4NPs, new bands at 1533 and 1412 cm^{-1} emerged, corresponding to the asymmetric and symmetric vibrational modes of a carboxylate stretching. Such results confirmed a bidentate mode of the coordination of the carboxylate functional group of Thc to Fe_3O_4NPs.[22,23]

The SEM shows the morphology of the CNC/Fe_3O_4NPs (Figure 2A). The deposition of AuNPs was then carried out to

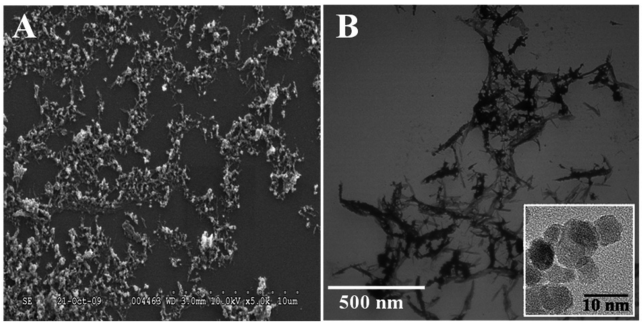

Figure 2. (A) SEM micrographs of CNC/Fe_3O_4NPs and (B) LVTEM image of CNC/Fe_3O_4NPs/AuNPs. Inset shows the HRTEM contrast and size difference between AuNPs (3−7 nm) and Fe_3O_4NPs (10−20 nm).

provide a high surface area for enzyme conjugation. $HAuCl_4$ was reduced with $NaBH_4$ in the presence of α-cyclodextrin to control the size of AuNPs in the CNC/Fe_3O_4NPs suspension. AuNPs were capped by free endocyclic disulfide groups of Thc to form the magnetite nanocomposite, CNC/Fe_3O_4NPs/AuNPs.[24] No significant change in the FTIR spectrum of CNCs/Fe_3O_4NPs/AuNPs was noticed. The product was separated from the reaction mixture with a magnet (shown in the inset of Scheme 1). The stable and uniform dispersion of Fe_3O_4NPs and AuNPs on CNCs was then confirmed by the LVTEM micrograph as shown in Figure 2B. AuNPs (3−7 nm in diameter) are darker than the 10−20 nm Fe_3O_4NPs as

dx.doi.org/10.1021/am4007534 | ACS Appl. Mater. Interfaces 2013, 5, 4978−4985

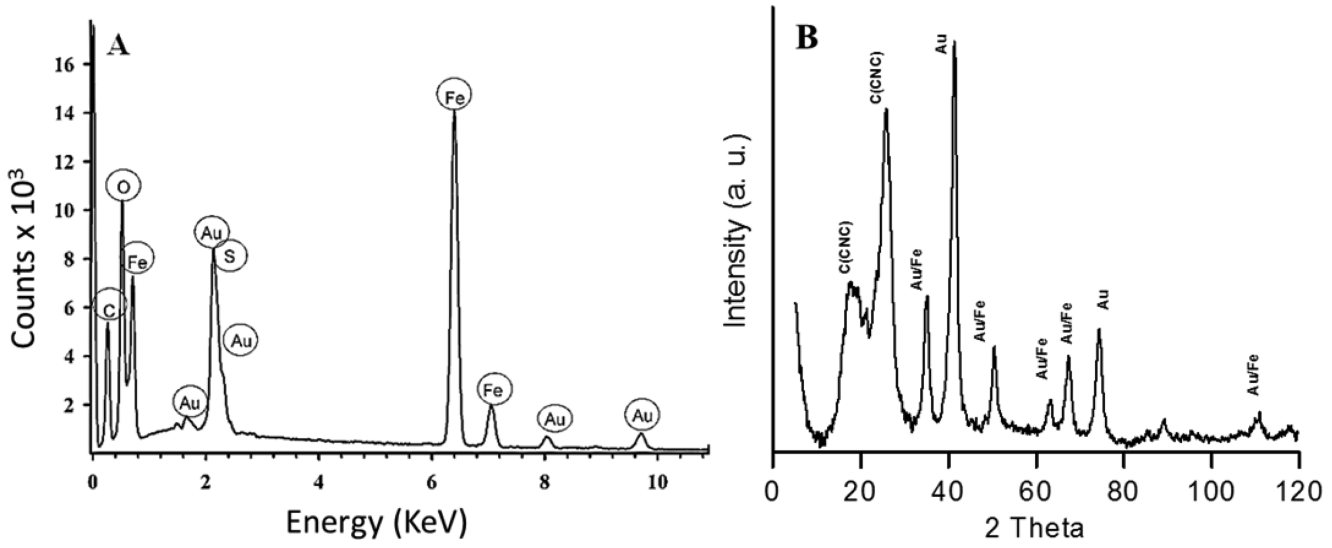

Figure 3. (A) EDX and (B) XRD representative spectra of CNC/Fe_3O_4NPs/AuNPs.

observed in the HRTEM micrograph (Inset, Figure 2B) because Au has a higher electron density compared to Fe_3O_4.[10,25] CNCs could not be probed by HRTEM because of a great difference in contrast between CNCs and metallic NPs on the carbon grid.

The elemental composition of the composites was determined by EDX as shown in Figure 3A and Table 1. The

Table 1. Elemental Analysis (atomic %) of the Different Composites

sample	C	O	N[a]	S	Fe	Au
CNC/Fe_3O_4NPs	44.9	46.4	n.d.	4.0	4.8	n.d.
CNC/Fe_3O_4NPs/AuNPs	44.1	50.2	n.d.	1.8	3.2	0.7
CNC/Fe_3O_4NPs/AuNPs/papain	45.9	41.3	8.8	1.1	2.5	0.4

[a]n.d. = not detectable.

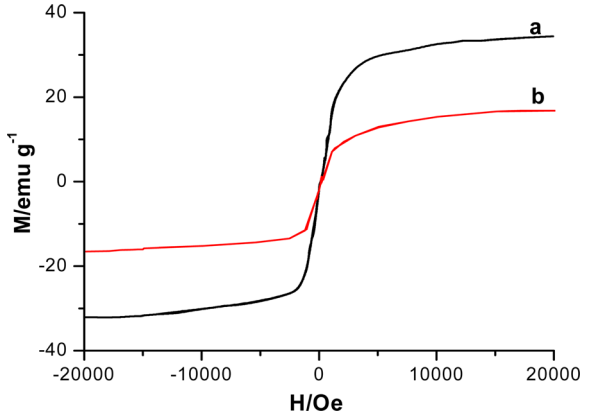

Figure 4. Room-temperature magnetic hysteresis curves for (a) CNC/Fe_3O_4NPs; (b) CNC/Fe_3O_4NPs/AuNPs.

Fe and Au signals confirmed the presence of both AuNPs and Fe_3O_4NPs, with S signals from Thc. The calculated molecular composition closely matched the composition of the starting materials within 3% standard deviation. Further evidence for the proposed elemental composition of the conjugate was confirmed by XRD (Figure 3B). The characteristic diffraction peaks of CNC were located at 2θ = 18 and 26°.[26] The diffraction peaks for Fe overlapped with the Au diffraction peaks.

The magnetic permeability of CNC/Fe_3O_4NPs, before and after the deposition of AuNPs, was evaluated by a vibrating sampling magnetometer at room temperature. The magnetic saturation value of CNC/Fe_3O_4NPs/AuNPs was reduced to 14.62 ± 0.09 emu g^{-1} as compared to 31.05 ± 0.11 emu g^{-1} for CNC/Fe_3O_4NPs (Figure 4).

Enzyme Conjugation and Electrochemical Protein Separation Assay. Papain was used as a model enzyme to test the efficiency of the CNC/Fe_3O_4NPs/AuNPs matrix as a reusable enzyme carrier that would not reduce the immobilization yield. Papain has been used in a variety of applications including cell isolation, cosmetics, food, pharmaceuticals, and textiles.[27,28] Various approaches have been attempted for the immobilization of papain to enhance the enzymatic activity, lifetime, and stability of the enzyme. Supports including mesoporous silica,[29] molecular sieves,[30] anion exchange resins,[31] polymeric beads,[32,33] and chitosan-modified magnetic nanoparticles.[28] To facilitate enzyme coupling, we introduced carboxylic acid groups to the CNC/Fe_3O_4NPs/AuNPs by coupling Thc to the AuNP surface via Au−S bonding, followed by NHS/EDC activation at pH 6.4. The second equivalent of Thc preferentially binds to the AuNPs of CNC/Fe_3O_4NPs/AuNPs through the disulfide group, leaving the carboxylic acid functionality free for further reactivity in enzyme immobilization. Papain covalently binds to the activated CNC/Fe_3O_4NPs/AuNPs matrix by the nucleophilic attack of amino groups on the activated COONHS groups. New characteristic bands at 1638 and 1546 cm^{-1} emerged, representing amide I and amide II stretches of the protein (Figure 1D).[28] From the EDX analysis, there was a change in the elemental composition of CNC/Fe_3O_4NPs/AuNPs/papain after enzyme binding where 8.8% nitrogen was introduced compared to CNC/Fe_3O_4NPs/AuNPs (Table 1). The masking effect of the enzyme occupying surface likely resulted in the reduction of Fe and Au content reported.

The enzyme loading capacity was evaluated by incubating papain (0.1−6.4 mg/mL) with activated CNC/Fe_3O_4NPs/AuNPs (10, 25, and 50 mg/mL). After the magnetic separation of the bound enzyme, the amount of unbound enzyme in the

supernatant was estimated by the Bradford assay to quantify the binding efficiency. With 10 mg of CNC/Fe_3O_4NPs/AuNPs as the support matrix, a 94% enzyme binding efficiency was achieved upon the addition of 1.2 mg/mL free enzyme (Figure 5). The percentage of bound enzyme decreased to 38.5% at 4.6

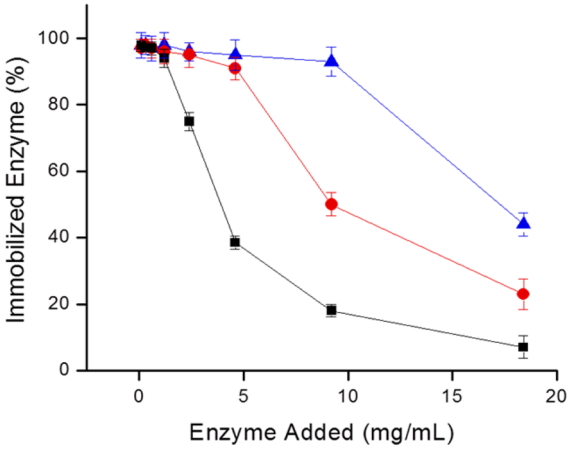

Figure 5. Enzyme binding efficiency of papain on the support matrix. Papain was added to 10 (■), 25 (●), and 50 (▲) mg/mL of the CNC/Fe_3O_4NPs/AuNPs supporting matrix.

mg/mL of added enzyme. When the supporting matrix was increased to 25 mg, the enzyme loading increased to 95% at 2.4 mg/mL of added enzyme. The highest papain loading was achieved by using 50 mg/mL CNC/Fe_3O_4NPs/AuNPs where 9.3 mg/mL free enzyme was immobilized on the support matrix for a 94% binding efficiency. Under these conditions, a papain loading of 186 mg/g of the support matrix was achieved, i.e., over 3-fold improvement from previously reported values.[34,35] This improvement in the enzyme loading could be attributed to a higher loading of AuNPs on the CNC/Fe_3O_4NPs/AuNPs matrix. Therefore, 50 mg CNC/Fe_3O_4NPs/AuNPs was preferred for this enzyme concentration range. No appreciable enzyme was released from the support matrix after extensive washing of the conjugated pellets.

A selective electrochemical screening assay was performed to test the conjugate as a protein receptor for enzyme purification. In brief, an Au electrode modified with the peptide film was used as a specific inhibitory probe for papain.[20] To ensure a well-packed self-assembled monolayer (SAM) on the electrode surface, we immersed the peptide film in decanethiol/ethanol solution for 2 min. The electrochemical response of the film due to the specific binding with papain in CNC/Fe_3O_4NPs/AuNPs/papain was evaluated by CV measurements in the papain activation buffer at pH 6.2 containing 2 M $NaClO_4$ as the supporting electrolyte. The films exhibited a single fully reversible one-electron redox peak with a formal potential E^0 of 0.459 ± 0.005 at 0.1 V s^{-1} vs Ag/AgCl. As expected, a positive shift of the formal potential and decrease in current was observed when the papain concentration was increased to 1.6 mg/mL (Figure 6A). Beyond this concentration, the potential reached steady state with a surface saturation of CNC/Fe_3O_4NPs/AuNPs/papain.

Figure 6B shows the CV response of the modified electrode after exposure to papain with and without CNC/Fe_3O_4NPs/AuNPs. The formal potential shifted +30.0 mV upon the addition of 0.5 mg/mL of free papain. After allowing the enzyme to react with the activated CNC/Fe_3O_4NPs/AuNPs, the potential shifted slightly to a higher potential as the enzyme immobilized on the matrix. When the suspension was exposed to a magnetic field, the formal potential shifted back 29.0 mV due to the magnetite matrix separation from the immobilized enzyme. Exposing the modified electrode to the support matrix without the enzyme only resulted in a current decrease without any significant potential shift. The Bradford assay confirmed that about 95% of the enzyme was bound to the matrix during the reaction.

DPV was used to evaluate the enzyme activity of the immobilized papain after in situ conjugation with the Fe_3O_4 nanocomposite. Figure 7A shows the change in the formal potential ΔE° as a function of the added papain concentration. Under the optimized conditions, a linear increase was obtained for an enzyme loading of 156 mg/g CNC/Fe_3O_4NPs/AuNPs before stabilizing at 86% retention of the active enzyme on the supporting matrix (Figure 7B).

Activity Assay of Free and Immobilized Enzyme. Free and immobilized papain enzymes were also assayed with the chromogenic substrate Z-Phe-Arg-NHNp. The Michaelis–Menten constant (K_m) was determined by monitoring the total papain-catalyzed hydrolysis of Z-Phe-Arg-NHNp catalyzed by free papain and CNC/Fe_3O_4NPs/AuNPs/papain at a high

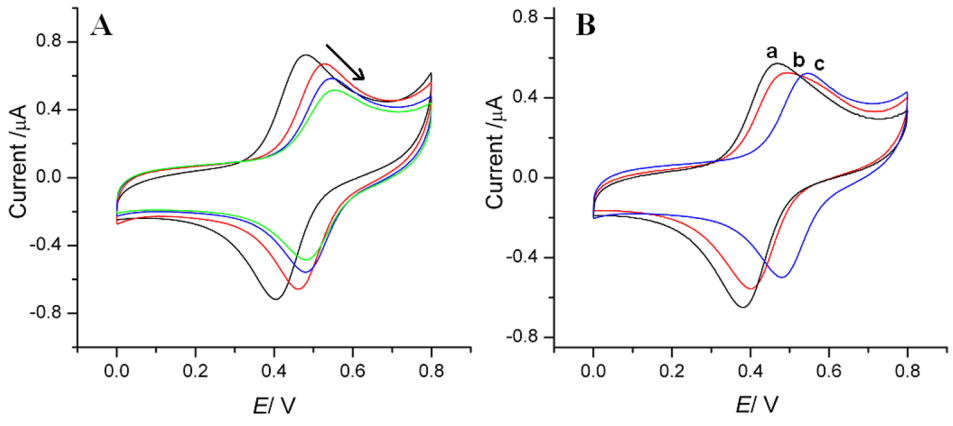

Figure 6. (A) CV of the Au electrode modified with Thc-Fca-Gly-Gly-Tyr-Arg and decanethiol in an activation buffer and increasing concentration of papain (0 (black), 0.4 (red), 0.8 (blue), 1.6 (green) mg/mL); (B) CV response of the modified electrode after exposure to 0.5 mg/mL papain (a) with, (b) without 50 mg CNC/Fe_3O_4NPs/AuNPs, and (c) after exposure to external magnet. Enzyme activation buffer (0.1 M sodium phosphate at pH 6.2, 2.5 mM EDTA, 300 μM DTT, and 30% DMSO, 23 °C) with 2 M $NaClO_4$. Scan rate of 0.1 V s^{-1}, Pt counter, Ag/AgCl reference.

dx.doi.org/10.1021/am4007534 | ACS Appl. Mater. Interfaces 2013, 5, 4978–4985

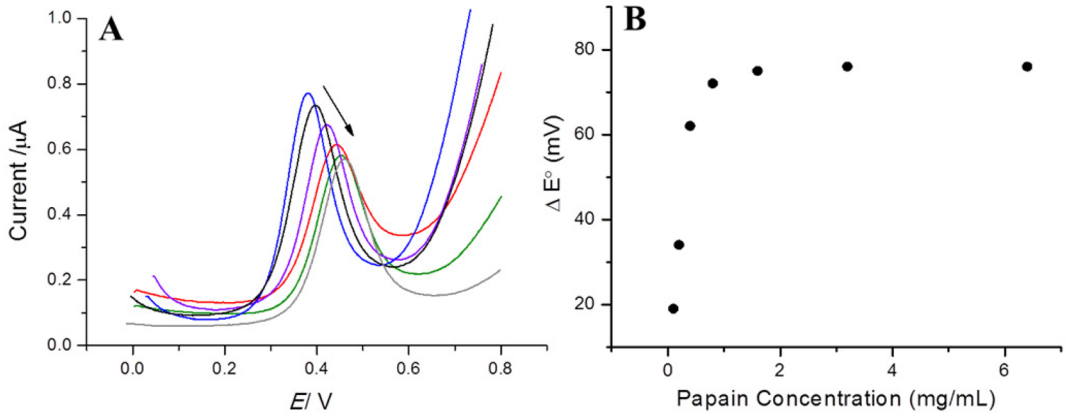

Figure 7. (A) DPV of the Au electrode modified with Thc-Fca-Gly-Gly-Tyr-Arg and decanethiol in an activation buffer detecting the binding efficiency of increasing concentration of papain (0.1−6.4 mg/mL) in the presence of 50 mg CNC/Fe_3O_4NPs/AuNPs supporting matrix. (B) Plot of the formal potential (E°) vs papain concentration.

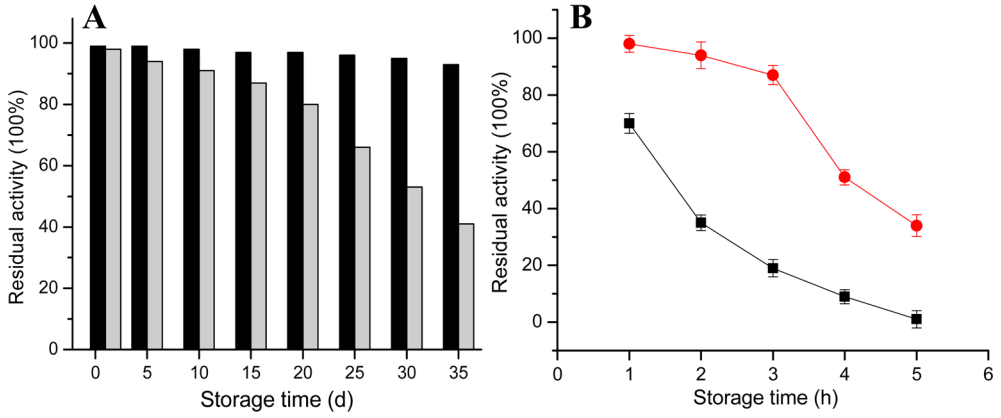

Figure 8. (A) Effect of storage time on the activity of immobilized (black) and free (light gray) papain. CNC/Fe_3O_4NPs/AuNPs/papain was prepared based on 9.6 mg/mL initial papain loaded on 50 mg/mL CNC/Fe_3O_4NPs/AuNPs. (B) Effect of storage temperature on the activity of free (■) and immobilized (●) papain at 70 °C. The total duration of the experiment was 5 h.

initial concentration of the substrate. The K_m value was determined at pH 6.2 by nonlinear regression of the concentration velocity curve using Michaelis−Menten equation ($\nu = \nu_{max}[S]/(K_m + [S])$, where ν is the velocity, ν_{max} is the maximum velocity, and [S] is the substrate concentration. The K_m value of immobilized and free papain was 1159 and 968 μM, respectively which compares well with the previously reported value for papain of 965 ± 244 μM.[36] Immobilized papain requires a higher substrate concentration compared to free papain under identical conditions which can be translated to 16% loss of the original activities. The reduced activity of the immobilized enzyme obtained from spectrophotometric and electrochemical assays could be attributed to protein molecules blocking active sites that prevent substrate interaction[37] or the reorientation of active sites after immobilization. These results validate the results obtained from the electrochemical experiment.

Effect of Storage Time and Temperature. After 35 days of storage at 4 °C, the immobilized enzyme retained 95% of its initial activity as compared to 41% for its free-form counterpart (Figure 8A). Thermal stability was examined by storing free and immobilized enzyme at 70 °C in PBS (pH 7.5), and the activity variations was assayed as described above. The immobilized and free enzyme retained 78 and 19% activity of the original value after 3 h, respectively (Figure 8B). The higher stability of papain conjugated with CNC/Fe_3O_4NPs/AuNPs are most likely due to the stabilization of papain molecules on the MNPs which is expected to improve the thermal tolerance of the immobilized enzyme as compared to the free counterpart.[28,38] The high surface area provided by the CNC/Fe_3O_4NPs/AuNPs conjugate may favor high binding capacity and high catalytic specificity of the conjugated enzyme.[39,40] Moreover, the small size and nonporosity of the support nanoparticles may allow papain molecule to expand over the nanoparticle surface with a better exposure of the active-site groove. It seems that immobilization induces conformational changes in three-dimensional structure of the enzyme through a series hydrogen bonds and hydrophopic interactions leading to higher stability as compared to the free counterpart.[41]

Recovery and Reuse of Immobilized Papain. Further investigation was focused on the reusability of the CNC/Fe_3O_4NPs/AuNPs/papain conjugate. The enzyme retained more than 80% of its initial activity after 12 cycles of magnetic separation and reuse under the same activity assay conditions (Figure 9). The decrease in activity could be attributed to gradual leakage of papain from the CNC/Fe_3O_4NPs/AuNPs matrix, loss of particles during magnetic separation, and/or enzyme denaturation.

dx.doi.org/10.1021/am4007534 | ACS Appl. Mater. Interfaces 2013, 5, 4978−4985

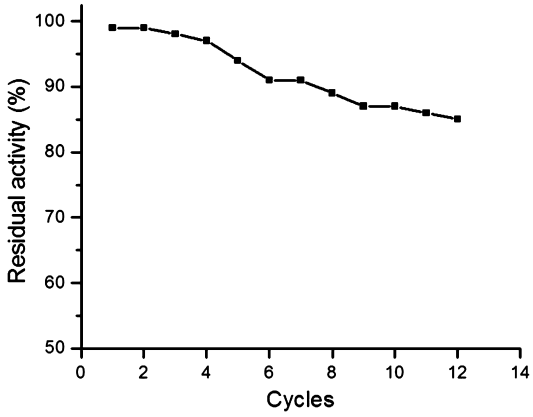

Figure 9. Residual activity of immobilized papain after repeated cycles of magnetic separation and reuse. The reaction was initiated by addition of the enzyme (20 μL) to catalyze the conversion of 200 μM Z-Phe-Arg-NHNp at 1−2 μM/min. CNC/Fe_3O_4NPs/AuNPs/papain was prepared based on 9.6 mg/mL initial papain loaded on 50 mg/mL CNC/Fe_3O_4NPs/AuNPs. The total duration of the experiment was 14 h.

CONCLUSION

This work has described the synthesis and characterization of Fe_3O_4NPs and AuNPs stabilized on CNCs. The CNC/Fe_3O_4NPs/AuNPs nanocomposite was used as a support matrix for the immobilization and separation of papain from the reaction solution with a maximum enzyme loading of 186 mg protein/g CNC/Fe_3O_4NPs/AuNPs. The conjugated material retained its high enzyme activity and demonstrated good stability and reusability. The facile electrochemical detection scheme provides a cheap and efficient alternative for evaluating the catalytic activity of the immobilized enzyme. On the basis of electrochemical detection and conventional spectrophotometric assay of the specific enzyme binding to the Thc-Fca-Gly-Gly-Tyr-Arg inhibitory film, the immobilized enzyme on CNC/Fe_3O_4NPs/AuNPs retained more than 83% of the original activity as compared to its free form, with significant thermal tolerance and reusability compared to the free counterpart. This work revealed magnetized CNCs as an efficient support matrix with great potential to serve as superior supports for enzymes, proteins, and other biomaterials.

AUTHOR INFORMATION

Corresponding Author

* E-mail: kmahmoud@qf.org.qa. Fax: +974 44541528.

Notes

The authors declare no competing financial interest.

ACKNOWLEDGMENTS

This work was supported in part by Canada's National Bioproducts Program. We thank Mr. D. Wang (ICPET, NRC, Canada) for the HRTEM analysis, Dr. John Tse of the Department of Physics and Engineering Physics, University of Saskatchewan, for the PXRD analysis and Mr. Ahmed Ramadan of Qatar University.

REFERENCES

(1) Bao, J.; Chen, W.; Liu, T.; Zhu, Y.; Jin, P.; Wang, L.; Liu, J.; Wei, Y.; Li, Y. *ACS Nano* **2007**, *1*, 293−298.
(2) Wang, J.; Bhattacharyya, D.; Bachas, L. G. *Biomacromolecules* **2001**, *2*, 700−705.
(3) Krogh, T. N.; Berg, T.; Højrup, P. *Anal. Biochem. Anal. Biochem.* **1999**, *274*, 153−162.
(4) Varlan, A. R.; Sansen, W.; Loey, A. V.; Hendrickx, M. *Biosens. Bioelectron.* **1996**, *11*, 443−448.
(5) Lei, H.; Wang, W.; Chen, L.-L.; Li, X.-C.; Yi, B.; Deng, L. *Biosen. Bioelectron.* **2004**, *35*, 15−21.
(6) Harris, L. A.; Goff, J. D.; Carmichael, A. Y.; Riffle, J. S.; Harburn, J. J.; St. Pierre, T. G.; Saunders, M. *Chem. Mater.* **2003**, *15*, 1367−1377.
(7) Laurent, S.; Forge, D.; Port, M.; Roch, A.; Robic, C.; Vander Elst, L.; Muller, R. N. *Chem. Rev.* **2008**, *108*, 2064−2110.
(8) Zhao, X.; Cai, Y.; Wang, T.; Shi, Y.; Jiang, G. *Anal. Chem.* **2008**, *80*, 9091−9096.
(9) Xu, Z.; Hou, Y.; Sun, S. *J. Am. Chem. Soc.* **2007**, *129*, 8698−8699.
(10) Yu, H.; Chen, M.; Rice, P. M.; Wang, S. X.; White, R. L.; Sun, S. *Nano Lett.* **2005**, *5*, 379−382.
(11) Mahmoud, K. A.; Male, K. B.; Hrapovic, S.; Luong, J. H. T. *ACS Appl. Mater. Interfaces* **2009**, *1*, 1383−1386.
(12) *Polysaccharide Materials: Performance by Design*; American Chemical Society: Washington, D.C., 2009; Vol. *1017*; pp i−v.
(13) Dong, S.; Roman, M. *J. Am. Chem. Soc.* **2007**, *129*, 13810−13811.
(14) Mahmoud, K. A.; Mena, J. A.; Male, K. B.; Hrapovic, S.; Kamen, A.; Luong, J. H. T. *ACS Appl. Mater. Inter.* **2010**, *2*, 2924−2932.
(15) Chen, X.; Li, J.; Li, X.; Jiang, L. *Biochem. Biophys. Res. Commun.* **1998**, *245*, 352−355.
(16) Vertegel, A. A.; Siegel, R. W.; Dordick, J. S. *Langmuir* **2004**, *20*, 6800−6807.
(17) Xiao, Y.; Ju, H.; Chen, H. *Anal. Chim. Acta* **1999**, *391*, 73−82.
(18) Liu, Z.-M.; Xie, C.; Wang, H.-Y.; Wu, P.; Meng, W. *J. Func. Mater.* **2012**, *43*, 1627−1631.
(19) Marchessault, R. H.; Brenmner, G.; Chauve, G. *ACS Symp. Ser.* **2006**, *934*, 3−17.
(20) Mahmoud, K. A.; Kraatz, H.-B. *Chem.—Eur. J.* **2007**, *13*, 5885−5895.
(21) Hayashi, K.; Moriya, M.; Sakamoto, W.; Yogo, T. *Chem. Mater.* **2009**, *21*, 1318−1325.
(22) Frimpong, R. A.; Hilt, J. Z. *Nanotechnology* **2008**, *19*, 1−7.
(23) Willis, A. L.; Turro, N. J.; O'Brien, S. *Chem. Mater.* **2005**, *17*, 5970−5975.
(24) Roux, S.; Garica, B.; Bridot, J. L.; Salom, M.; Marquette, C.; Lemelle, L.; Gillet, P.; Blum, L.; Perriat, P.; Tillement, O. *Langmuir* **2005**, *21*, 2526−2536.
(25) Robinson, I.; Tung, L. D.; Maenosono, S.; Walti, C.; Thanh, N. T. K. *Nanoscale* **2010**, *2*, 2624−2630.
(26) Leung, A. C. W.; Hrapovic, S.; Lam, E.; Liu, Y.; Male, K. B.; Mahmoud, K. A.; Luong, J. H. T. *Small* **2011**, *7*, 302−305.
(27) Amri, E.; Mamboya, F. *Am. J. Biochem. Biotechnol.* **2012**, *8*, 99−104.
(28) Liang, Y.-Y.; Zhang, L.-M. *Biomacromolecules* **2007**, *8*, 1480−1486.
(29) Solís, S.; Paniagua, J.; Martínez, J. C.; Asomoza, M. *J. Sol−Gel Sci. Technol.* **2006**, *37*, 125−127.
(30) Zhao, B.; Shi, B.; Ma, R. *Eng. Life Sci.* **2005**, *5*, 436−441.
(31) Chiou, R. Y. Y.; Beuchat, L. R. *J. Food Biochem.* **1987**, *11*, 163−176.
(32) Hayashi, T.; Hirayama, C.; Iwatsuki, M. *J. Appl. Polym. Sci.* **1992**, *44*, 143−150.
(33) Hayashi, T.; Ikada, Y. *Biotechnol. Bioeng.* **1990**, *35*, 518−524.
(34) Sahoo, B.; Sahu, S. K.; Bhattacharya, D.; Dhara, D.; Pramanik, P. *Colloid Surfaces B* **2013**, *101*, 280−289.
(35) Wang, A.; Wang, H.; Zhou, C.; Du, Z.; Zhu, S.; Shen, S. *Chin. J. Chem. Eng.* **2008**, *16*, 612−619.
(36) Loser, R.; Schilling, K.; Dimmig, E.; Gutschow, M. *J. Med. Chem.* **2005**, *48*, 7688−7707.
(37) Clark, D. S. *Trends Biotechnol.* **1994**, *12*, 439−443.
(38) Ren, Y.; Rivera, J.; He, L.; Kulkarni, H.; Lee, D.-K.; Messersmith, P. *BMC Biotechnol.* **2011**, *11* (63), 1−8.

(39) Konwarh, R.; Karak, N.; Rai, S. K.; Mukherjee, A. K. *Nanotechnology* **2009**, *20*, 225−235.
(40) Johnson, A. K.; Zawadzka, A. M.; Deobald, L. A.; Crawford, R. L.; Paszczynski, A. J. *J. Nanopart. Res.* **2008**, *10*, 1009−1025.
(41) Ansari, S. A.; Husain, Q. *Biotechnol. Adv.* **2012**, *30*, 512−523.